Continuous, Tract-Constrained Directional Vector Fields from rDCM Effective Connectivity Using Mixture Density Networks

Wiktor Tomasik
Independent Researcher

09.01.2026

Abstract

Effective connectivity estimates from dynamic causal modeling (rDCM) are typically represented as dense directed matrices. However, these matrices do not directly specify a continuous, geometric description of how directed influence is routed through 3D white matter anatomy. Because these estimates are expressed as abstract parcel to parcel weights, they may require fusion with additional data, such as diffusion MRI tractography in order to define anatomically plausible pathways. I present a solution for fusing whole-cortex estimates from regression dynamic causal modeling (Schaefer-400) with a dense tractography atlas (HCP-1065). The method computes streamline path histograms to filter directed streamline micro-segments ("teacher segments") based on rDCM values, training a mixture density network to learn a smooth 3D vector field over brain continuum space. The MDN serves as both a fusion mechanism and a continuous summary of dominant directional patterns, addressing the interpretability challenge of dense raw tractography. Validation is reported at three levels: (A) global diagnostics, (B) local directional agreement between the MDN and teacher segments, and (C) parcel-wise diagnostics comparing MDN field metrics with rDCM asymmetry and entropy measures. The learned field matches the teacher geometry strongly (MDN vs. teacher cosine similarity 0.961). However, parcel-level correlations with rDCM metrics are weak ($|r| \lesssim 0.1$). This divergence suggests that the geometric constraints imposed by white matter anatomy exert a dominant influence that cannot be captured by Euclidean vector approximations of effective connectivity. DMN parcels exhibit lower input and output entropy than non-DMN parcels ($p < 0.002$), consistent with more concentrated flow under this proxy. Overall, the learned field closely reproduces the teacher geometry but highlights the non-trivial geometric mismatch between matrix-level connectivity and continuous anatomical routing.

1 Introduction

Directed connectivity methods such as dynamic causal modeling aim to infer effective connectivity directed influences among brain regions – from fMRI time series[1]. These methods provide a scalable formulation that can estimate whole-brain directed effective connectivity across many regions, enabling analyses at the scale of modern cortical parcellations[2]. However, rDCM outputs are typically represented as dense directed matrices. These matrices do not directly express how directed influences might be related to continuous space, or how white matter anatomy constrains plausible routes[3]. Diffusion MRI tractography provides an anatomical approximation of white-matter pathways. While tractography does not encode directionality of information transfer by itself, it provides plausible geometric conduits. A natural idea is therefore to fuse directed effective connectivity estimates over parcels with streamline geometry, producing a tract constrained geometric proxy for directed "flow". In this research, "flow" is used strictly as an approximation and should not be read as a direct biophysical claim about neural signal propagation. The central challenge is that once effective connectivity is fused with whole-brain tractography, the resulting output is extremely dense and difficult to interpret. Additional step is needed to smooth out and summarize dominant, consistent directions while retaining spatial continuity.

Here I propose and evaluate a pipeline that:

- uses rDCM effective connectivity over the Schaefer-400 parcellation,
- associates these directed edge weights with streamlines from an HCP-1065 whole-brain tractography atlas,
- converts weighted, directed streamline fragments into a large "teacher" dataset, that consist of micro-segments with local direction targets, and
- trains a mixture density network (MDN) to learn a continuous 3D vector field that best explains these directed micro-segments.

MDNs are well suited because multiple plausible local directions can coexist at the same location in white matter. By predicting a mixture of Gaussians over local displacement vectors the model can represent complex direction distributions but still providing a smooth field for visualization.

The main contribution of this work is a practical, reproducible framework for converting parcel-level directed connectivity into a continuous field constrained by anatomical geometry.

2 Data and Resources

2.1 Effective connectivity (rDCM) and parcellation

Effective connectivity matrices were obtained as precomputed rDCM-derived directed connectivity matrices defined on the Schaefer-400 cortical parcellation[4].

In this study, these matrices are treated as fixed inputs used to inform construction of the teacher micro segments and also diagnostics for validation. The Schaefer parcellation provides a widely used functional atlas with multiple resolutions, including 400 parcels.

2.2 Structural geometry (tractography)

White matter geometry was taken from the HCP-1065 whole-brain tractography atlas[7], used here as a dense set of streamlines. These streamlines provide the 3D geometric substrate used for the teacher micro segment representation.

All spatial coordinates used for MDN training and export are in the tractogram world coordinate convention. Streamlines are provided in MNI space (mm), and we use that same coordinate system for all exported grids.

2.3 Dataset sources used in this work

Connectivity sources: rDCM effective connectivity matrices derived from datasets including MICA-MICs and HCP (Schaefer-400 parcellation)[5, 6].

Tractography source: Data from the Human Connectome Project (n=10).

3 Dataset generation

3.1 Dataset

rDCM input: Precomputed directed effective connectivity matrix

$$A \in \mathbb{R}^{400\times 400}$$

on Schaefer-400. In this pipeline, A is used upstream to fuse directed parcel-to-parcel weights with tractography geometry by constructing an rDCM-weighted directed streamline micro-segment dataset "teacher segments". To be more specific, for each directed parcel pair $(i \to j)$ with weight A_{ij}, streamlines consistent with that parcel pair are converted into many small directed fragments; fragments are oriented in the $i \to j$ direction and retained/weighted according to A_{ij} (via streamline path histograms used for filtering and selection). The resulting supervised dataset stores local segment endpoints and displacement targets.

During MDN training, A can additionally be used as an optional local conditioning feature (Section 3.3). This conditioning is a bonus feature and is not required for the learned field to reflect rDCM, because the rDCM–tractography fusion is already encoded in the teacher segments themselves.

Tract geometry: HCP-1065 tractography atlas streamlines in tractogram world coordinates.

Teacher segment dataset: Training is performed using teacher dataset whose rows include `SEG_P0`, `SEG_P1`, and `V0` (and optionally `W`, and optionally `ROI_I/ROI_J`

and NB_IDX/NB_W). Each row represents one directed micro segment SEG_P0→SEG_P1 with supervision target.

$$\Delta S = V_0 \in \mathbb{R}^3.$$

Generated teacher dataset consists of these fields:

Edge-to-streamline association Directed rDCM edges $(i \to j)$ with weights A_{ij} are mapped onto tractography by computing streamline path histograms. These histograms are used to select and weight streamline trajectories consistent with $(i \to j)$, in proportion to A_{ij}

Directed micro-segmentation (teacher rows used in the reported run). Each selected streamline is oriented to match the rDCM direction $(i \to j)$ and split into short directed fragments. For each fragment the script writes:

- SEG_P0, SEG_P1 (successive points along the oriented streamline; world coordinates), and
- V0 the local displacement target (typically SEG_P1 − SEG_P0)

Optional training weight. Per-row scalar W so that fragments supported by more reliable rDCM-weighted evidence contribute more strongly during MDN optimization.

Additional metadata required only for rDCM conditioning. If conditioning is enabled, the teacher must also provide NB_IDX and NB_W, which define a local neighborhood over parcels used at training time to form the mixed rDCM feature row $\tilde{A}(x)$ from A. Even when conditioning is disabled, the learned field remains rDCM-informed because the rDCM×tractography fusion is already encoded in which directed micro-segments are retained (and optionally how they are weighted) in the teacher artifact.

3.2 Training data sampling

For each teacher segment SEG_P0→SEG_P1, I sample

$$x = (1 - t)\,\mathrm{SEG\_P0} + t\,\mathrm{SEG\_P1}, \qquad t \sim \mathrm{Uniform}(0, 1),$$

with supervision target

$$\Delta S = V_0$$

(defined by the teacher as a 3D segment vector in tractogram coordinates)

Spatial jitter: small Gaussian jitter is applied to x, but not to the targets (V_0). During my testing jittering the targets was found to be detrimental, introducing degradation that outweighed any potential regularization benefits.

3.3 MDN model and objective

An MLP mixture density network is trained, mapping $x = (x, y, z)$ to a K-component Gaussian mixture for $\Delta S \in \mathbb{R}^3$ (diagonal covariances), with $K = 6$.

For each component k, the model outputs $\mu_k(x) \in \mathbb{R}^3$, $\sigma_k(x) \in \mathbb{R}^3$ (softplus + small floor), and mixing logits $\pi_k(x)$, with

$$\alpha_k(x) = \mathrm{softmax}(\pi(x))_k,$$
$$p(\Delta S \mid x) = \sum_{k=1}^{K} \alpha_k(x)\, \mathcal{N}\Big(\Delta S;\, \mu_k(x),\, \mathrm{diag}(\sigma_k(x)^2)\Big),$$

and loss

$$\mathcal{L}_{\mathrm{NLL}} = -\log p(V_0 \mid x).$$

Proposed architecture: rDCM conditioning: the pipeline supports extending the input from x to $[x \,\|\, \tilde{A}(x)]$, where $\tilde{A}(x) \in \mathbb{R}^{400}$ is a locally mixed rDCM row computed from teacher-provided neighborhood metadata (`NB_IDX`, `NB_W`):

$$\tilde{A}(x) = \sum_m \mathrm{NB\_W}_m \; A[\mathrm{NB\_IDX}_m, :].$$

Purpose: provide additional parcel-level directed context at each spatial location beyond xyz. Even when this conditioning is disabled, the MDN still learns an rDCM-informed field because supervision comes from the rDCM weighted directed teacher segments constructed upstream.

Proposed architecture: ROI embeddings. Training also supports embedding ROI indices (`ROI_I`, `ROI_J`) and concatenating them to the input to provide explicit parcel identity.

Experimental implementation: Stabilization used in the reported run:

- Entropy regularization on mixture weights $\alpha(x)$: coefficient λ is set to 1×10^{-2} initially and decreased to 0 over 5,000 training steps
- Logit temperature warmdown: $T : 1.8 \to 1.0$ over 4000 steps.
- Batching enforces coverage across z slices: 10 bins along z.
- Learning rate policy: $lr_{\min} = 5 \times 10^{-7}$, $lr_{\max} = 1 \times 10^{-3}$; LR finder then warmup + cosine for fixed 6-hour budget.

The MDN model provided in the supplementary data was trained using only xyz inputs at the MDN stage. rDCM conditioning and ROI embeddings were turned off, as they exceeded GPU memory limits at stable batch sizes

Diagnostics and validation

Because the MDN is trained on teacher vectors V_0 from spatial location x, the primary validation is teacher fidelity. rDCM-related tests are reported as exploratory consistency checks, since the reported model does not take rDCM features or ROI identity as inputs, and any agreement can only arise indirectly.

A) Teacher fidelity

Global direction. Cosine between normalized global sums (teacher vs MDN) is computed from sampled segments. The resulting value is reported in the Results section.

Local distribution. Sample teacher segments, evaluate $\bar{v}(x)$ at segment midpoints by trilinear interpolation on the exported grid, compute $\cos(\bar{v}, V_0)$, filter $\|V_0\| > 10^{-6}$, and report $\|V_0\|$-weighted summaries. The resulting summaries are reported in the Results section.

B) rDCM parcel validation

I compute a coarse per to parcel flux proxy from the exported mean field by sampling $\bar{v}(\cdot)$ on a sphere around each Schaefer 400 centroid and averaging outward normal dot products. In my run I used radius 6.5 mm and 1024 sphere directions; the directions are generated using a Fibonacci lattice sampler to approximate uniform coverage on the sphere.

I compare this flux proxy to parcel wise scalar summaries derived from the rDCM matrix A, including signed asymmetries between outgoing and incoming connections, asymmetries computed using only positive values, and measures of concentration and dispersion derived from entropy. Parcel-wise Pearson correlations are computed and reported in the Results section.

I additionally compare the MDN mean field near centroids to rDCM derived inward and outward direction vectors by constructing, for each ROI, a net outgoing vector as the weighted sum of directions from that centroid to other centroids with weights $\max(A_{ij}, 0)$, and an analogous incoming vector using $\max(A_{ji}, 0)$. I then summarize cosine similarities between $\bar{v}$ at the centroid and these rDCM direction vectors. The resulting summaries are reported in the Results section.

C) DMN network level validation

I include a DMN network level validation because the default mode network is a widely studied in large scale system in the Schaefer 400 / 17 network and is often discussed in terms of integrative, hub[8]. Here it provides a simple, interpretable network-level stratification for an exploratory check of the rDCM entropy proxies. Results are interpreted with caution.

Network labels. DMN membership is defined by a parcel network mapping generated from the Schaefer 400 / 17 network atlas labels. I then split parcels into DMN vs not DMN and compared their rDCM entropy value.

DMN vs rest entropy proxy Using DMN $N = 79$:

Input entropy and Output entropy are computed under this proxy and reported in the Results section.

4 Results

The trained MDN produces a continuous 3D vector field that, when visualized through particle advection, can reveal coherent macroscopic pathways and dominant directional trends that are difficult to discern in raw directed streamline visualizations. Compared to plotting all directed streamline connections, the MDN field acts as a spatially smooth summary that emphasizes consistent routes and down-weights rare or inconsistent micro-paths. This is a visualization and exploratory representation of the rDCM-informed, tract-constrained teacher construction, rather than a direct estimate of physiological signal transmission. Figure 1 provides a side-view rendering of the learned tract-constrained field under two visualization strategies.

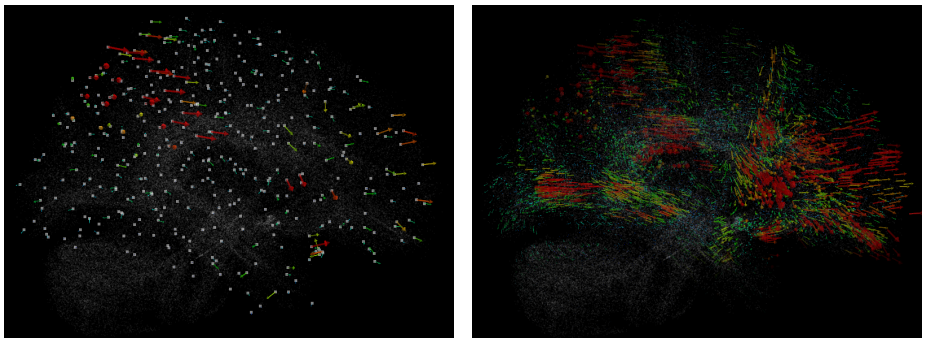

A ROI-seeded field visualization (rDCM parcels).

B Tract-seeded visualization with entropy-based opacity.

FIGURE 1 Visualization of the learned continuous vector field (MDN mean field) under two seeding strategies. **A:** Vectors are seeded only from the rDCM ROI support (Schaefer-400), showing directions restricted to the effective-connectivity ROI coverage. **B:** Vectors are seeded from tractography support points (whole-brain streamline geometry); vector opacity is modulated by voxelwise MDN mixture entropy (more transparent = higher entropy / lower confidence). This opacity masking is applied because tractography coverage and cortex-based rDCM ROI coverage are not identical, so confidence-weighting down-weights regions where the model is less constrained by rDCM-defined ROI support. In both panels, arrow color and length reflect vector magnitude.

Quantitatively, the main findings are:

High fidelity to the constructed teacher flow. Global MDN mean field direction matches the aggregate teacher direction with cosine 0.9610 (16.05°) over

3,766,806 sampled micro-segments (mean length 0.5106 mm). A per-segment cosine diagnostic further shows heterogeneous local agreement (19,000,000 sampled points; 4,382,035 retained after filtering $\|V_0\| > 10^{-6}$), with $\|V_0\|$-weighted median 0.5777 and p_{90} 0.9874.

Weak parcel-wise correspondence to simple rDCM summary proxies under current definitions. Parcel-wise correlations between the MDN flux proxy and rDCM asymmetry/entropy-derived measures are small ($|r| \lesssim 0.1$) in this run: flux vs asym_pos: +0.014; flux vs asym_signed: +0.025; flux vs input_concentration: +0.091; flux vs output_dispersion: −0.092. Centroid-direction comparisons between the local MDN mean field and rDCM-derived IN/OUT centroid vectors also show weak overall alignment (MDN(mean) vs rDCM OUT: median −0.081, mean −0.066; MDN(mean) vs rDCM IN: median +0.075, mean +0.068; with DMN/rest stratified medians as reported in the diagnostics).

DMN entropy differences indicate more concentrated rDCM partner distributions under the present proxy. At network level (DMN $N = 79$ parcels), DMN parcels show lower input and output entropy than the rest of cortex under the present entropy proxy: Input entropy: DMN 0.352 vs rest 0.377 ($t = -3.210$, $p = 0.00159$); Output entropy: DMN 0.351 vs rest 0.377 ($t = -3.743$, $p = 0.000239$). Under this proxy, lower entropy means the normalized incoming/outgoing weight distributions are less uniform, i.e. a smaller subset of source/target parcels accounts for a larger fraction of total incoming/outgoing weight.

5 Discussion

This study presented a pipeline for fusing rDCM effective connectivity with diffusion MRI tractography to generate continuous, tract-constrained directional vector fields. By training a Mixture Density Network (MDN) on rDCM-weighted "teacher" streamlines, I generated a smooth 3D field that respects white matter geometry. The high fidelity between the learned field and the teacher dataset (global cosine similarity > 0.96) demonstrates that the MDN successfully captures the complex routing of the training data. However, the divergence between this field and simple parcel-level summaries offers the most critical insights.

5.1 Anatomical Geometry vs. Euclidean Abstraction

A key finding is the weak correspondence between the learned field's local flux and rDCM-derived directional vectors ($|r| \lesssim 0.1$). This divergence highlights a fundamental property of structural connectivity: the geometry imposed by white matter streamlines exerts a dominant influence on flow that cannot be approximated by Euclidean displacement vectors.

While effective connectivity is often conceptualized abstractly as a weight between two nodes, attempting to visualize this as a direct linear path in 3D space is geometrically insufficient. The near-zero correlation indicates that the "routing" mechanisms of white matter are not merely fine-tuned versions of a straight trajectory, but are topologically distinct. Consequently, any attempt to visualize information flow in 3D without incorporating streamline geometry will likely misrepresent the spatial reality of signal transmission.

However, this dominance of geometry presents a limitation. The results suggest that the strong shape of the underlying tracts may overshadow the specific variance introduced by rDCM weights. Because the MDN prioritizes fitting the highly curved spatial constraints of the tractography, the resulting visualization is heavily biased toward structural connectivity. This implies that while the field is anatomically plausible, the current fusion method may need refinement to allow the effective connectivity weights to modulate the field more visibly, rather than just determining which tracts are included.

5.2 Network-Level Insights: DMN Concentration

Despite the strong anatomical constraints, the field successfully captured network-level topologies. Default Mode Network (DMN) parcels exhibited significantly lower input and output entropy compared to non-DMN parcels ($p < 0.002$). Under the defined proxy, this lower entropy indicates "concentration"—DMN nodes tend to exchange influence with a selective set of anatomical partners rather than dispersing flow uniformly. This aligns with the characterization of the DMN as an integrated core system and suggests that the pipeline preserves aggregate topological properties even when local vector correlations are noisy.

5.3 A Continuous Proxy for Connectivity

The MDN approach serves as a continuous compression algorithm, converting dense, overlapping streamlines into a coherent "weather map" of directional influence. This addresses the interpretability challenge of raw tractography by smoothing out inconsistent micro-segments and highlighting dominant routing patterns.

5.4 Limitations and Future Directions

The primary limitation of this work is the "geometry mismatch" described above. Because the structural influence is so strong, the learned field is a better proxy for tract anatomy than for the subtle variations in effective connectivity. Future work should investigate "advection-based" connectivity, where rDCM values are not just used to filter training data, but are dynamically verified by simulating particle flow through the generated field. Additionally, more sophisticated fusion techniques are needed to balance the contribution of tract geometry and rDCM weights, ensuring that the visualization reflects the func-

tional variance of effective connectivity as strongly as it reflects the structural constraints of white matter.

Ethics Statement

All human neuroimaging data used in this work were obtained from publicly available resources (Human Connectome Project and associated derived atlases/datasets). Ethical approval and informed consent procedures were handled by the original data providers as described in their publications and documentation.

Data Availability

We release three research artifacts:

- **Supplementary Movie:** a rendered particle-advection visualization through the exported MDN mean field. The animation is generated from the field evaluated on the full bounding-box grid for continuity of advection; therefore, motion may also appear in regions that are not covered by the cortex-based rDCM parcellation. A confidence-weighted rendering is illustrated in Figure 1**B**, where opacity is modulated by voxelwise MDN mixture entropy (more transparent = lower confidence).

- **Derived Dataset:** a precomputed 3D grid cache of the learned mixture vector field (resolution 125^3) and a support/seeding point cloud. The grid cache is stored as raw `float32` little-endian binary arrays, together with a JSON manifest that specifies the bounding box (MNI mm), grid resolution, array layout, and filenames. The cache includes (i) the mixture-mean field, (ii) per-component mean fields for all mixture components, (iii) mixture weights per voxel, and (iv) voxelwise mixture-entropy as an uncertainty proxy.

  Note: Because the effective-connectivity input is defined on a cortex-based parcellation (Schaefer-400), the exported bounding-box grid contains values outside the rDCM ROI coverage. For anatomical interpretation of "brain-shaped" structure, analyses and visualizations should be restricted to voxels overlapping the rDCM ROI support.

- **Trained Model :** PyTorch model weights for the final K=6 component mixture density network (MDN) vector-field model used to generate the released grid cache and movie.

Training data provenance. The model was trained using teacher supervision derived from publicly available neuroimaging resources, including whole-brain tractography (HCP-1065) and effective connectivity (rDCM; Schaefer-400 parcellation).

External datasets and resources.

- Schaefer parcellation (400 parcels): `https://academic.oup.com/cercor/article/28/9/3095/3978804`
- Human Connectome Project overview: `https://doi.org/10.1016/j.neuroimage.2013.05.041`
- MICA-MICs dataset paper: `https://www.nature.com/articles/s41597-022-01682-y`
- DSI Studio atlas releases (includes HCP-based tractography atlases): `https://github.com/frankyeh/DSI-Studio-atlas/releases`

References

[1] K. J. Friston, L. Harrison, and W. Penny. Dynamic causal modelling. *NeuroImage*, 19(4):1273–1302, 2003. doi:10.1016/S1053-8119(03)00202-7.

[2] S. Frässle et al. Regression dynamic causal modeling for resting-state fMRI. *Human Brain Mapping*, 42(7):2159–2180, 2021. doi:10.1002/hbm.25357.

[3] K. E. Stephan et al. Tractography-based priors for dynamic causal models. *NeuroImage*, 47(4):1628–1638, 2009. doi:10.1016/j.neuroimage.2009.05.096.

[4] A. Schaefer et al. Local-Global Parcellation of the Human Cerebral Cortex from Intrinsic Functional Connectivity MRI. *Cerebral Cortex*, 28(9):3095–3114, 2018. doi:10.1093/cercor/bhx179.

[5] J. Royer et al. An Open MRI Dataset For Multiscale Neuroscience. *Scientific Data*, 9:569, 2022. doi:10.1038/s41597-022-01682-y.

[6] D. C. Van Essen et al. The WU-Minn Human Connectome Project: An overview. *NeuroImage*, 80:62–79, 2013. doi:10.1016/j.neuroimage.2013.05.041.

[7] F.-C. Yeh et al. Population-based tract-to-region connectome of the human brain. *Nature Communications*, 13:4933, 2022. doi:10.1038/s41467-022-32595-4.

[8] R. L. Buckner, J. R. Andrews-Hanna, and D. L. Schacter. The brain's default network: anatomy, function, and relevance to disease. *Annals of the New York Academy of Sciences*, 1124:1–38, 2008. doi:10.1196/annals.1440.011.